Journal of Mechanics Engineering and Automation 13 (2023) 40-53
doi: 10.17265/2159-5275/2023.02.003

Methane Concentration Influence on Combustion in a Rapid Compression Machine under DFICE Relevant Conditions

R. Clemente-Mallada, A. Peter, S. Riess, L. Strauss, H. Fajri and M. Wensing

Fluid Systems Engineering, Friedrich-Alexander University, Cauerstrasse 4, Erlangen-Tennenlohe 91058, Germany

Abstract: In this experimental work, an optically accessible rapid compression machine is used to study the ignition and combustion process under engine relevant operation conditions for five different air-natural gas equivalence ratios (λ) ignited with either 12.2 mg or 6.7 mg of pilot diesel injected at 1,600 bar. Initial temperature of the ambient mixture, walls and injector was 333 K. Additionally, for the short (6.7 mg) diesel injection, the variation in the ID (ignition delay) for two higher ambient temperatures (343 K and 353 K) was measured. Pressure and piston displacement are recorded while two high-speed cameras simultaneously capture signals in the visible range spectrum and at 305 nm wavelength for OH* chemiluminescence respectively. ID is measured both from OH* and pressure rise. From the recorded data, the heat release ratio is estimated and compared with the visual signals. This gives an insight of the temporal and spatial evolution of the flame, as well as a qualitative perception of the transition from spray ignition into a premixed flame in the ambient fuel-air mixture. It was found that increasing the methane concertation delays the ignition, reduces the natural flame luminosity and enhances the OH* chemiluminescence signal.

Key words: Dual-fuel, natural gas, diesel, rapid compression machine, ID.

1. Introduction

Newer astringent legislations on environmental and health protection (EURO VI standards) foster research in seek of new concepts such as DFICEs (dual fuel internal combustion engines), a promising alternative for substituting heavy-duty diesel engines for off-road and stationary applications where electrification in the short term is not foreseen. DFICEs ignite by compression of a high-cetane number fuel to produce a pilot flame that results in the ignition of a high-octane number fuel-air-mixture. This kind of RCCI (reactivity controlled compression ignition, for a deep review on the topic refer to Reitz and Duraisamy [1]) turns to be of interest for real operation as a low temperature combustion strategy: lean-high-octane-number fuel-air blends reduce maximum combustion temperature peaks avoiding NO_x and non-equilibrium pollutants whereas it maintains the thermal efficiency and torque typical for diesel engines. The high-octane number fuel can be liquid or gas. For liquid fuels, near zero NO_x and soot emissions have been achieved by a diesel engine modified to operate with gasoline/diesel as in the work of Ma et al. [2]. Although, there are studies on ignition strategies for liquid fuels alternative to the dual fuel combustion such as prechamber ignition [3], homogeneous charge compression ignition [4] or doping the high-octane fuel with cetane number improvers [5]. Nevertheless, DFICEs (dual fuel internal combustion engines) are a more mature and robust technology, especially when it comes to gaseous fuels. Natural gas lean mixtures can cause quenching leading to high-unburnt hydrocarbons emissions. In example, for methane the limiting lean equivalence ratio that supports complete combustion is $\Phi \sim 0.5$ whereas for hydrogen it is $\Phi \sim 0.1$. Moreover, when dealing with natural gas, the mixture reactivity becomes

Corresponding author: Rafael Clemente Mallada, MSc, research field: dual fuel combustion.

highly sensitive to the concentration of *n*-butane [6]. Using natural gas in a dual fuel configuration not only allows operating with leaner mixtures but also provides high knock-resistance and carbon dioxide emission reduction [7]. In the case of DFICEs that use natural gas as substitution fuel it is of vital importance to correctly understand the combustion mechanism in order to assure a complete methane combustion: unburnt methane is estimated to have a global warming potential ranging from 25 to 36 over a 100-year time-lapse. To study the narrow band of air-natural gas mixture composition that avoids the methane slip at low engine loads is still a challenge for which the recent numerical study of Mikulski et al. [8] gives a positive prospect. So does the optical investigation in a 200 mm bore marine engine of Merts et al. [9] in which the indicated efficiency of a RCCI does not suggest a highly incomplete methane combustion while a significant amount of the camera's pixels have a visual signal level not higher than background noise, which could be explained by a low soot production. Eventually, low particle emissions of dual fuel combustion could enable strategies of water port injection to improve further the thermal efficiency as investigated by Chen et al. [10]. In this work, a rapid compression machine is used to study the ignition and combustion processes for natural-gas/diesel mixtures.

2. Experimental Setup and Measurement System

All experiments took place in a pneumatically driven rapid compression machine, which is optically accessible and can control the natural gas equivalence ratio. The piston compresses a preloaded blend of air and natural gas at 2 bar and 333 K. Later, a pilot diesel fuel is injected into the combustion chamber so ignition occurs close to TDC (top dead center). All the numbers used for the description of the experimental rig in this section refer to the sketch of Fig. 1, an adaptation from Refs. [11, 12]. Most typical application field of rapid compression machines is to study chemical kinetic mechanisms or the ID (ignition delay) as in the works of Desantes et al. [13, 14] or Kobori et al. [15] rather than imitating the complete thermodynamic cycle of a reciprocating engine. Nonetheless, Srna et al. [7, 16-18] already used this kind of experimental device to recreate the conditions of a DFICE that uses natural gas as substitution fuel as an analogy to study the auto-ignition and the combustion mode transition from a spray diffusive flame into a premixed flame front propagation.

2.1 The Rapid Compression Machine

The experimental rig is a RCM (rapid compression machine) manufactured by TESTEM GmbH (https://testem.de). This device is not driven by a crack-shaft mechanism. Instead, the working principle of the device is based on a simultaneous and opposite movement of two masses which are hydraulically coupled to each other. These two masses are, on the one hand, a driving piston or mass compensation piston (1) and, on the other hand, the connecting rod tube (2) attached to the working piston (3). Before the start of compression, pressurized air at 39 bar is blow through two vents (4) so the driving piston (1) is compressed against the oil reservoir (5). The working piston is located 200 mm away from the cylinder top wall resting on the diaphragm (6) so that the pressurized oil volume (5) is initially divided into two. With these initial locations of the piston and driving pressure, researchers aim to measure a maximum piston displacement of 195 mm as stroke. The cylinder bore is 84 mm. Accounting for an additional volume of approximately 55.4 cm^3 from the ensemble of the RCM piston's window (7), RCM's methane injection tubes downstream the check valves (8) and the exhaust conduct (9), an effective volumetric pressure ratio of $\frac{v_{max}}{v_{min}} = \varepsilon = 14:1$ is obtained. In order to initiate the compression a solenoid valve-controlled bypass connecting the two initial oil volumes (10) is released. Then the pressurized oil begins to flow into the left side of the diaphragm (6) slowly pushing

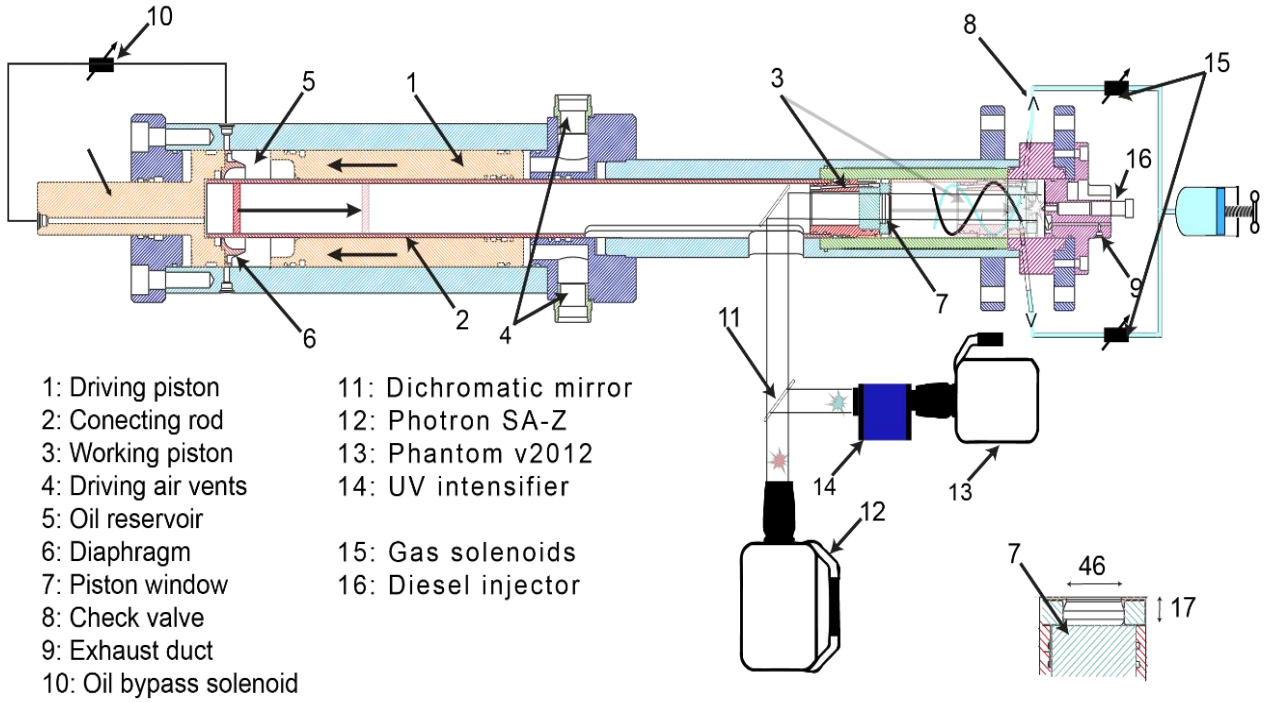

Fig. 1 Sketch of the experimental setup. Adapted from Refs. [11, 12].

the connecting rod tube (2) out of the gap. As soon as the end of the connecting rod tube (2) passes over the radial sealing ring of the gap the oil can enter the interior of the connecting rod unhindered delivering a rapid compression process. The latter rapid compression process lasts less than 6 ms as shown by pressure trace in Fig. 2. RCM can record the piston displacement with an accuracy of 0.01 mm and there is a piezoelectric pressure transducer (Kistler typ 6045A) mounted in the cylinder head to measure the pressure evolution. As in the work of Srna et al. [17, 18] pressure trace is filtered by mean of a Savtitzky-Golay filter with a polynomial order of 3 and a frame length of 11.

2.2 Optical Measurement Equipment

For optical investigation OH* and natural luminosity two high speed cameras were available to record a window of 512×512 pixels at a framerate of 100 kHz with a projected pixel size of 0.2 mm. Light beam separation is done using a dichromatic mirror (11) with a high pass wavelength above 320 nm. That means a camera assembly of 90° between each other. A Photron FASTCAM SA-Z type 2100K-M camera (12) was used for recording natural luminosity. Ultraviolet imaging for OH* takes place with a UV filtered intensified high-speed imaging camera Phantom v2012 equipped with a Nikon UV-Nikkor 105 mm f = 4.5 objective (13). Filter bandpass is 307±25 nm and the UV signal was enhanced by an Intensified Relay Optic IRO-X S20 from LaVision (14). Intensifier gate was set to 18,000 ns and gain to 66%.

2.3 Fuel and Injection

As diesel fuel, a bio-diesel free reference fuel (CEC Legislative Fuel RF-06-03) was used. As high octane number fuel, a mixture in volume of 95.3% methane and 4.7% propane, which represents a methane number of 80, was chosen from the work of Peter et al. [19] to represent natural gas. Spray plumes and injection flow rate were characterized following the same work. After each measurement, RCM would scavenge the combustion products. After scavenging the cylinder and placing the piston at its initial location, the RCM would seal its exhaust duct (9). Then, two solenoid

valves (15) would open to charge the combustion chamber of 200 mm length, 84 mm diameter (l/*d* = 2.38) in two steps. First, the natural gas and second the air slowly fill up the cylinder volume at BDC (bottom dead center). A continental AG V1376 piezo-hydraulic diesel research injector (16) with three nozzles of nominal diameter 115 μm (l/*d* = 6.5) arranged with an elevation angle of 45° with respect the injector symmetry axis and an umbrella angle of 90° delivers the pilot diesel fuel straight into the volume of the piston's window (7). To characterize this injector, firstly its flow rate was measured with an HDA-500 device from Moehwald GmbH. For this injector, when energization time is below 500 μs, injection takes place during the ballistic region of the nozzle. Thus, flowrate is transient due to the short energization time. Secondly, inert Schlieren photography and Mie Scattering measurements were carried out in a preheated and pressurized optically accessible chamber at pressure and temperature conditions representative of those at RCM's top dead center. Spray angle and penetration depth were obtained following ECN (engine combustion network) directions [20]. Mie liquid length turned to be about 22 mm proving complete spray evaporation halfway between injector tip and wall. From the measured cone angle, air entrainment was approached following Naber and Siebers law [20]. The good fitting of the cone angle gives the authors confidence about the injector discharge coefficient, $c_d = 0.84$ and velocity coefficient, $c_v = 0.89$ (area contraction coefficient, $c_a = 0.94$). In order to achieve ignition at the same cylinder position in the RCM, a pulse delay generator (Quantum Composer 9520) adjusts the SOI (start of injection) among different λ variations with the objective of maintaining the ignition around 195 mm away from the piston's initial position. This is achieved by delaying the electrical start of injection from the moment piston reaches 180 mm, as gathered in Table 1. The delays gathered in Table 1 were obtained by try and error in previous experiments. SOI occurs between 1.5 and 2.5 ms before top dead center whereas in the work of Srna et al. [7, 16-18] SOI is 3.5 ms before TDC. Thus, in these experiments, mixing and ignition processes have to take place in a 60% to 30% shorter time span. As shown in Table 1, in the present work, the energy content of the pilot fuel as a percentage of the total fuel energy ranges from the 6% (for the richest methane ambient content $\lambda = 1.5$) to the 20% ($\lambda = 3.0$). Therefore, the current experiments do not belong to the category of micro-pilot injections, which typically applies to pilot injections that represent less than 2% of the total energy. This constitutes a major difference with the work of Srna et al. [17, 18] that using a single hole injector does fall in such a category although the injection durations in this work are very similar (270 μs and 430 μs).

3. Heat Release

Heat liberated through combustion, can be determined from the measured pressure and volume values at RCM if given a model to account for the heat losses, that is heat transferred from the bulk gas into the wall and the work of the friction force between the piston and the combustion chamber. To quantitatively account heat losses in the RCM Srna et al. [17] modified the average cylinder gas velocity in Woschni's heat transfer coefficient so it accounts properly for the heat losses during natural gas combustion. In the present work, authors chose to use an effective polytrophic index as in Eq. (5) of the work of Wissink and Reitz [21] about RCCI of diesel-gasoline. The idea is to interpolate such polytropic index with a logistic function between the values of the polytropic indexes that adjust compression and the expansion strokes. In order to bring some light to this, Fig. 2 presents an example of a recorded pressure trace as a continuous black line, $\hat{p}$. Vertical black lines indicate the hydraulic injection of fuel, obtained from the results of the measured in the quantity and rate measuring unit HDA-500 which allowed measuring a 275 μs delay between the electrical start of injection and the actual flowing of the fuel out of the nozzles. Alike, blue vertical lines

represent the duration of the OH* chemiluminescence signal using the 10% threshold criteria explained in Section 4. Knowing the volume ratio for each position of the piston and the initial volume, a polytropic evolution (blue dotted line, $\hat{p}_{comp}$) was fitted into the compression stroke between the start of the rapid compression and the start of injection obtaining n_{comp}. Similarly, to obtain exp , a polytropic process was fitted between the end of the OH* signal and the bottom dead center (red dotted line, $\hat{p}_{exp}$). Wissink and Reitz [21] logistic function is defined in a crank angle domain, but the nature of the RCM oblige us to model the transition with a sigmoid function,

$$n = n_{comp} + \frac{n_{exp} - n_{comp}}{1 + e^{-\tau}} \quad (1)$$

under a relaxation time,

$$\tau = 10\left(\frac{t - t_{p_{rise}}}{2\,(t_{PHHR} - t_{p_{rise}})} - \frac{1}{2}\right) \quad (2)$$

Table 1 Experimental conditions sum up of the nine different cases (six long injections and three short injections of diesel)

λ [1]	∞	3	2.6	2.2	1.8	1.5
Φ [1]	0	0.33	0.38	0.45	0.55	0.66
m_{gas}	0	45.8	52.6	61.7	74.7	94.7
m_{diesel}	12.2; 6.7	12.2	12.2	12.2; 6.7	12.2; 6.7	6.7
x_{O_2} [1]	0.21	0.202	0.201	0.199	0.197	0.195
x_{CH_4} [1]	0	0.04	0.046	0.054	0.066	0.08
x_{N_2} [1]	0.79	0.756	0.755	0.749	0.741	0.732
Subs. [1]	0	4.1	4.7	5.5; 11	6.6; 13.1	15.4
Delay [μs]	1,900	1,550	1,500	1,400	1,200	900
d_{SOI} [mm]	192±0.7	190.0±0.7	190±0.60	190±0.60	190±0.1	187±0.3
d_{ig} [mm]	195.1±0.9	195.4±0.8	195.4±0.8	195.5±0.6	195.7±0.6	195.6±0.4

λ and Φ: Air/natural-gas and natural-gas/air mixture equivalence ratio; m_{gas}: target gas mass in ambient; m_{diesel}: mass of the pilot injection; Substitution: ratio between energy content of the methane and the pilot fuel; x_{O_2}, x_{CH_4} and x_{N_2}: molar fractions; Delay: time span between the moment when the piston reaches 180 mm away from the piston's start position and SOI and time and piston displacement at start of injection and ignition; d_{SOI} and d_{ig}: piston distance from start position.

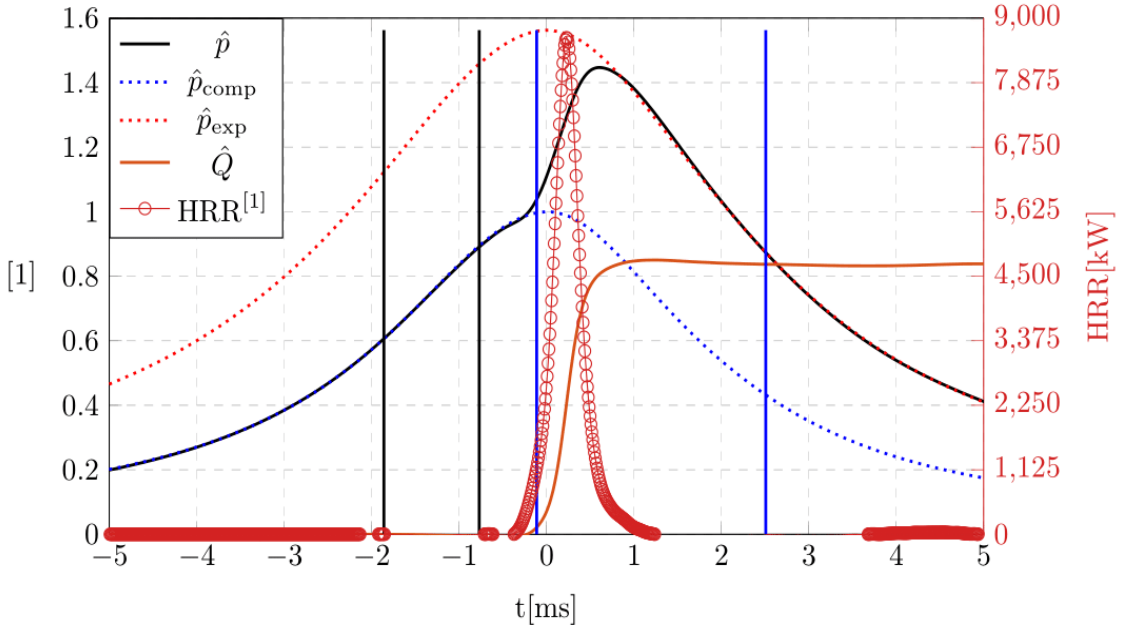

Fig. 2 Pressure trace and HRR calculation for an experiment of λ = 1.8 ignited with a 12.2 mg diesel injection whose duration is indicated by the two vertical black lines. Blue vertical lines stand for the duration of OH* signal.

In expression 2, $t_{p_{rise}}$ is the time when a pressure increase is detected, as defined in Section 4. t_{PHHR} is the time when the peak of the heat release rate (red line with circular markers, HRR) takes place and has to be calculated iteratively as in the work of Wissink and Reitz [21]. The time integration of this HRR works as an estimation of the cumulative heat released during the combustion, $\hat{Q}$. Pressures in Fig. 2 are expressed in non-dimensional times of the maximum pressure of the polytropic compression process. Likely, in this plot cumulative HRR appears divided by lower calorific power of the diesel and natural gas used in the experiment.

This non-dimensional cumulative HRR can be thought as an indicator of the combustion efficiency for each natural gas concentration, depending on the amount of pilot fuel as in Fig. 3, where marks correspond to each experiment and lines represent the mean value plus minus one standard deviation. Flame does not propagate in the lean mixture act and the low combustion temperature seems to produce an unburnt natural gas emission of up to two thirds of the initial charge, but rich mixtures achieve a combustion efficiency as high as the single fuel diesel cases. As happened in the experiments of Srna et al. [17], a smaller ignition source reduces efficiency, but this effect can be compensated employing richer mixtures.

The high variation in the efficiency results for each case can be due to the low initial temperature of 60 °C. To visualize the evolution of the reaction zones during combustion, contour lines ranging from 50% to 100% of the high temperature chemiluminescence intensity maximum value during the peak of the heat release ratio were overleaped with the averaged OH* images in Fig. 4. In the diesel case it is easy to observe how, the recirculation zones established as result of the interaction of two sprays plumes concentrate the highest number of OH* chemiluminescence counts. Two factors might contribute to that. On the one hand, a higher local initial temperature from the diesel combustion in these recirculation zones and then new natural gas arrive because of convection into these hot spots. On the other hand, OH* is an intensive signal integrated in the direction of the camera, because of angular momentum conservation of the fluid a vortex stretching effect lengthening the recirculation areas might accelerate the advance of flame front through the ambient mixture in the transversal direction. Also, OH* is clearly visible outside the recirculation zones as well. The fact that for the leanest case a black area without OH* signal appears in the centre of the combustion chamber leads to the hypothesis that, in order to achieve a good and complete combustion of the ambient natural gas the high temperature conditions that first appear in the

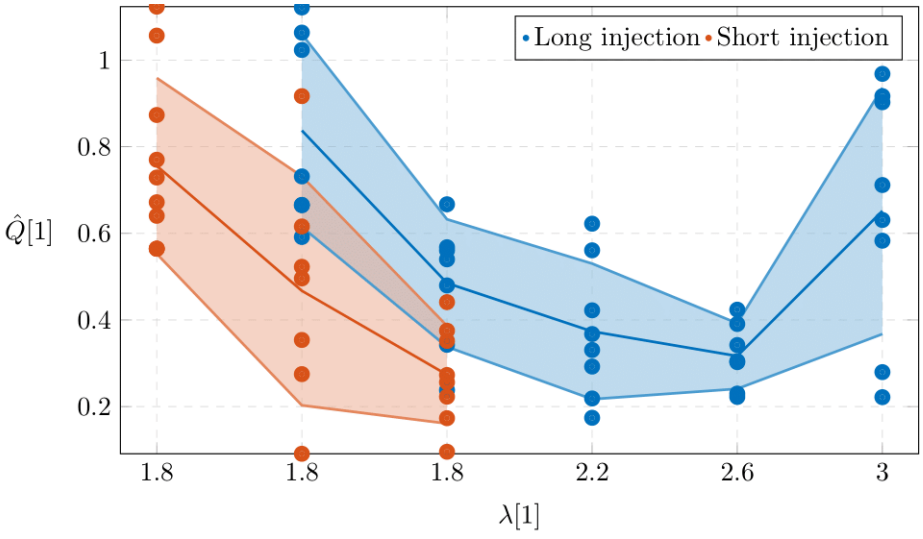

Fig. 3 Combustion efficiency.

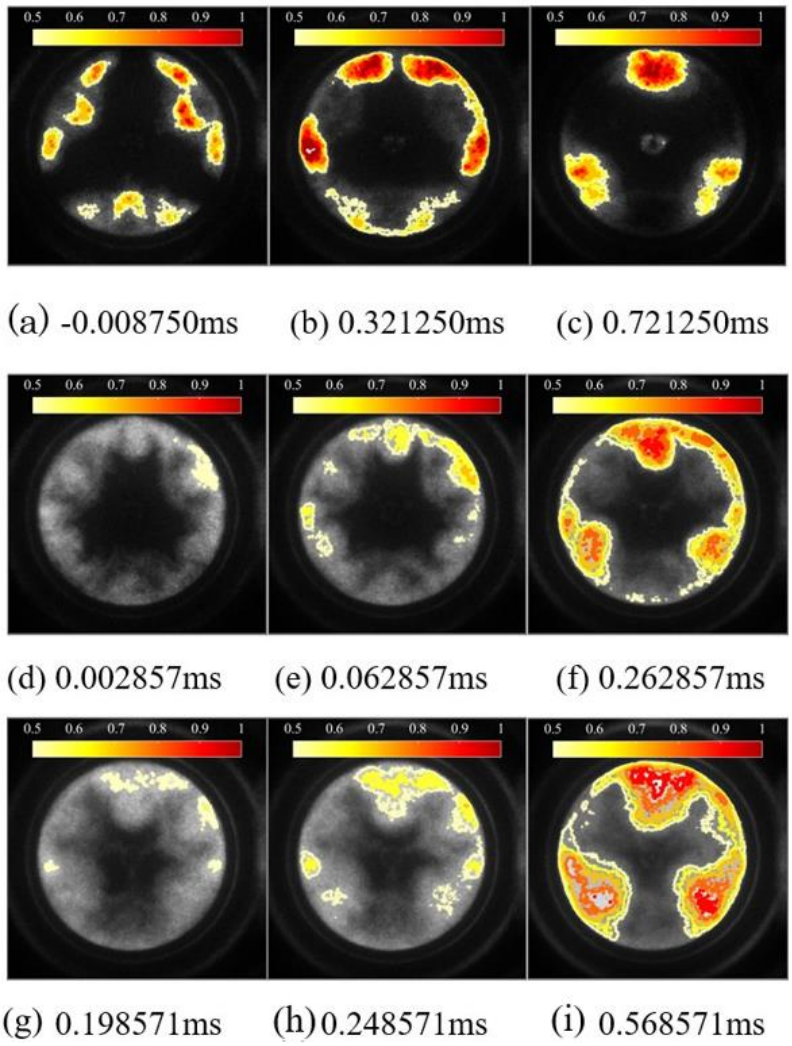

Fig. 4 OH* chemiluminescence snapshots for pure air (top row), λ = 3.0 (middle row) and λ = 1.8 (bottom row) ignited with a 12.2 mg of reference diesel pilot injection. Origin of times (0 ms) corresponds to TDC. Contour-lines range from 50% to 100% of the maximum OH* level at PHRR. Subfigures (a), (d) and (g) correspond to the earliest time stamp with any area showing OH* chemiluminescence signal above 50% of the maximum, indicating a self-sustained combustion of the natural gas. Subfigures (c), (f) and (i) correspond with the PHHR.

kernel of the pilot flame must last long enough for the premixed methane flame to propagate towards the centre of the cylinder. A too lean and not fast enough reaction will not compensate the enthalpy balance against the wall heat losses and the expansion work.

4. Ignition

Traditionally the literature tells apart a cold combustion from a hot combustion in the ignition and in the reaction zones of any hydrocarbon flame. During the cold combustion, the largest molecules break down into more reactive spices to initiate the high-temperature combustion associated with the large amount of energy liberated when hydrogen atoms split their bonds with other molecules. Whereas the most representative chemistry of a cold combustion is the formation of formaldehyde (CH_2O) [22], the hot combustion regions are characterized for the consumption of CH_2O and the production of radical hydroxyl (OH*). Regarding the high-temperature ID, Srna et al. [17, 18] use both the rapid rise of the HRR and a threshold in the OH* chemiluminescence as an

indicator. As it is appreciable in Fig. 2, when adjusting a tangent line to the HRR curve to obtain the ID from the intersection of such line with the abscissas as in the work of Srna et al. [17] provides a slightly (less than 1 ms) earlier ID than the 10% OH* criteria. About the low-temperature ID, Skeen et al. [23] tell how several research groups have used high-speed schlieren imaging to visualize low-temperature ignition processes in sprays: as a cascade of reactions liberate heat, the spray's refractive index gradient softens and the schlieren signal briefly disappears. However, the same work highlights that the earliest softening of the schlieren effect happens some tens of microseconds after the first formaldehyde formation. In the present work, a cold combustion ID was estimated from the pressure trace as the difference in time between the eSOI (electrical start of injection) and the point in time when the pressure trace rises a 1% above the polytropic compression curve. Unlike in the work of Pickett et al. [24] this ignition time was not corrected to account for delay of the order of 0.1 ms due to the speed of sound as Lillo et al. [25] propose. Low temperature ID for the 12 mg diesel injection is presented in Fig. 5 by red circles. Due to the smaller pressure rise, it was not possible to apply this 1% threshold criterion consistently for the short diesel injection. Reader should keep in mind that the earliest expansion of the spray associated to such pressure rise happens later than the schlieren transparency so this should be considered a late low temperature reaction indicator. Likewise, hot temperature combustion ID was measured as the timespan between eSOI and the moment corresponding to the first frame of the high speed OH* chemiluminescence camera in which the optical counts sum up a 10% of maximum OH* glowing intensity for each recording. This threshold criteria is in fashion of the ECN work [25]. In Fig. 5, blue circles in the domain between $\lambda = 1.8$ and $\lambda = \infty$ stand for the high temperature ignition in the long diesel injection cases. It is interesting how the low temperature and the high temperature ID of these experiments keep a quite constant distance. Blue triangles in the domain of Fig. 6 between $\lambda = 2.2$ and $\lambda = 1.5$ represent the hot temperature ID for the short pilot injection of 6.2 mg cases. The fact that short and long injections present similar ID for $\lambda = 1.8$ and $\lambda = 2.2$ and the visualization of OH* images leads the authors to suggest that this particular threshold criteria, for these experiments is actually measuring the start of the high temperature reaction in the natural gas. This idea agrees with the observation of Srna et al. [17] about how the simultaneous combustion of natural gas entrained in the pilot-spray volume increases the PHRR associated to the combustion of the pilot fuel.

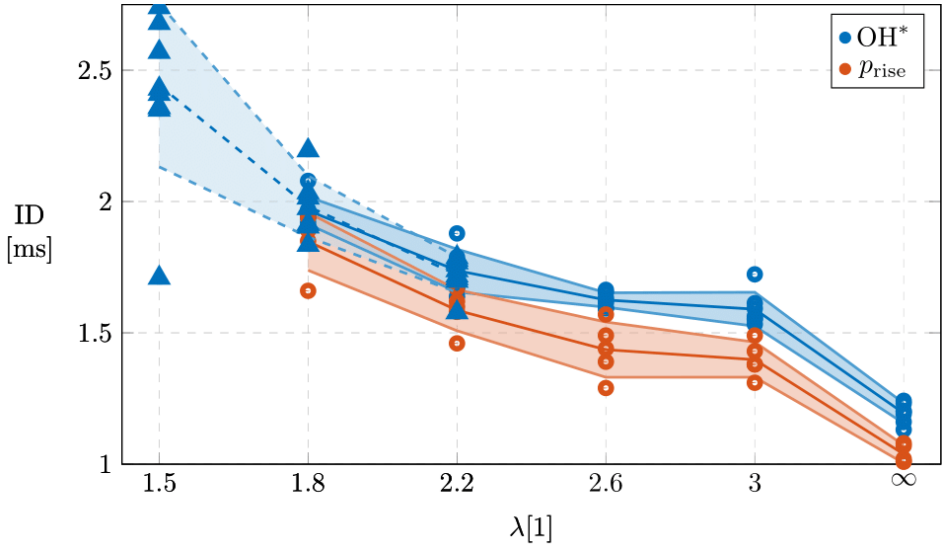

Fig. 5 ID. Lines present average plus/minus one standard deviation.

4.1 Ignition and Natural Gas Concentration

In an attempt for achieving some qualitative results in the ID from the OH* chemiluminescence, the role of the of methane chemical properties reactivity as a surrogate of natural gas was analysed with single step chemistry. In fact, although it may result counterintuitive, methane turns to have a flame inhibitor behaviour: When modelling its combustion through a single step chemistry mechanism with a pseudo-first-order reaction rate constant,

$$k = AT^n \exp\left(\frac{-E_a}{RT}\right)[Fuel]^a[Oxidizer]^b \qquad (3)$$

the exponential coefficient for methane turns to be negative [26]. On the other hand, the ambient methane displaces oxygen molecules reducing its concentration and complicating the ignition of diesel spray. It is good here to drag our attention to two works from SANDIA NL in which an Arrhenius-type expression is used to correlate ID data for diesel sprays. On the one hand, Idicheriay and Pickett [27] do it in terms of the oxygen concentration to study the ID for different EGR levels. On the other hand Pickett et al. [24] tell apart the effects of ambient density and oxygen concentration from different stoichiometric mixture fractions, Z_{st}. To look into the possibility of taking account for the effects of substituting oxygen with methane a variation of these expressions was proposed as follows:

$$\tau_{\mathrm{ID}} \sim A\rho_{\mathrm{O_2}}^{l}\rho_{\mathrm{d}}^{m}\rho_{\mathrm{CH_4}}^{n}\exp\left(\frac{E_a}{RT}\right) \qquad (4)$$

As the ambient molar fractions: x_{O_2}, x_{CH_4} and x_{N_2} are known for each methane/air mixture equivalence ratio; under the strong assumptions that ignition occurs for stoichiometric air-fuel ratio of dodecane and methane as diesel and natural gas surrogates, the simplified reaction is:

$$\mathrm{C_{12}H_{26}} + \nu\mathrm{CH_4} + \left(\frac{37}{2} + 2\nu\right)\mathrm{O_2} + \mu\mathrm{N_2} \rightarrow\rightarrow \mathrm{CO_2} + \mathrm{H_2O} + \mu\mathrm{N_2} \qquad (5)$$

where $\nu = \frac{37}{2}\frac{x_{\mathrm{CH_4}}}{x_{\mathrm{O_2}} - 2x_{\mathrm{CH_4}}}$ and thus, because the ambient density at the ignition time (ρ_{a}) is known, partial densities in Eq. (4) can be estimated from their spices molar fraction as: $\rho_{\mathrm{d}} \simeq \rho_{\mathrm{a}}\frac{1}{\nu+\left(\frac{37}{2}+2\nu\right)+\mu}$, $\rho_{\mathrm{CH_4}} = \rho_{\mathrm{a}}\frac{\left(\frac{37}{2}+2\nu\right)}{1+\nu+\mu}$ and $\rho_{\mathrm{O_2}} = \rho_{\mathrm{a}}\frac{\nu}{1+\mu}$. Now, by rewriting Eq. (4) with logarithms,

$$\ln(\tau_{\mathrm{ID}}) \sim \ln\left(\rho_{\mathrm{O_2}}^{l}\rho_{\mathrm{d}}^{m}\rho_{\mathrm{CH_4}}^{n}\right) + \ln(A) + \frac{E_a}{RT} = ax + b \qquad (6)$$

it shows that, under the assumption of a single step Arrhenius reaction, the rate of change of the ID could be trimmed into a linear regression. The abscissa of such regression (x-axis) corresponds to the rate of change of the inverse of and the inverse of an "effective" density, $\ln\left(\rho_{\mathrm{O_2}}^{l}\rho_{\mathrm{d}}^{m}\rho_{\mathrm{CH_4}}^{n}\right)$.

A constant (b) gathers the huge importance of temperature in the reaction initiation. Any non-unitary slope, $(a \neq 1)$, implies that the concentration exponents (l, m, n) used to define such "effective density" are not valid because there is no factor premultiplying the logarithm. Note than when modelling the reaction speed as in Eq. (3), the concentration exponents for diesel and oxygen are positive (they accelerate the reaction) and the opposite for methane. Their sings change when talking about time (ID). The concentration exponent for calculating the reaction rate constant compiled in the work of Westbrook [26] for long alkanes is 0.25. Because it is expected that the flame inhibitor behaviour of the methane plays a smaller role in the auto-ignition of the diesel to auto ignite, the concentration exponent of the methane was raised from -0.3 [26] to -0.2. Oxygen concertation exponent was arbitrarily assigned 0.9 so the product would maintain the physical dimensions of density. Fig. 6 represents the ID for the different ambient natural gas/air mixture equivalence ratio against the inverse of an "effective" density, $\left(\rho_{\mathrm{O_2}}^{-0.9}\rho_{\mathrm{d}}^{-0.3}\rho_{\mathrm{CH_4}}^{0.2}\right)$ in double

logarithmic axis, a graphical equivalent to Eq. (6). The black straight overleaped to the chart has slope unity. Square and diamond markers correspond to the long and short pilot fuel injection respectively. The ten and eight arm stars correspond with the two variations into higher temperatures of the initial charge which imply a much higher temperature after compression. It is a good sign that these two temperature variations seem to fall within a line parallel to the black line of slope unity that adjusts the 333 K original family of experiments. Approximately, the increment of 10 K and 20 K in the initial temperature corresponds, respectively, to an increment of 3% (about 10 K) and 6% (about 20 K) of the ambient temperature at TDC before ignition. Thus, approximately, temperatures before ignition are 660 K, 680 K and 700 K. In agreement with the work of Srna et al. [17, 18], the two different injection strategies (long and short pilot injection) do not have any effect in the ID above or at least, it is smaller the data dispersion due to temperature and concentration uncertainty. Bullet marks with error crosses added over the experiment marks correspond to the ID calculated with CANTERA (https://cantera.org/) as the time where the net production of OH* is maximum for the simulation of an ideal gas reactor object as mass and volume in the RCM are known and temperature can be estimated adjusting a polytropic process to the compression stroke as $\hat{p}_{comp}$ in Fig. 2. The used reaction mechanism used was the C1-C16 HT + Soot + NO_x reaction mechanism developed by the Creck Modelling Group from Politecnico di Milano [28-30] considering *n*-dodecane as surrogate for the diesel pilot fuel.

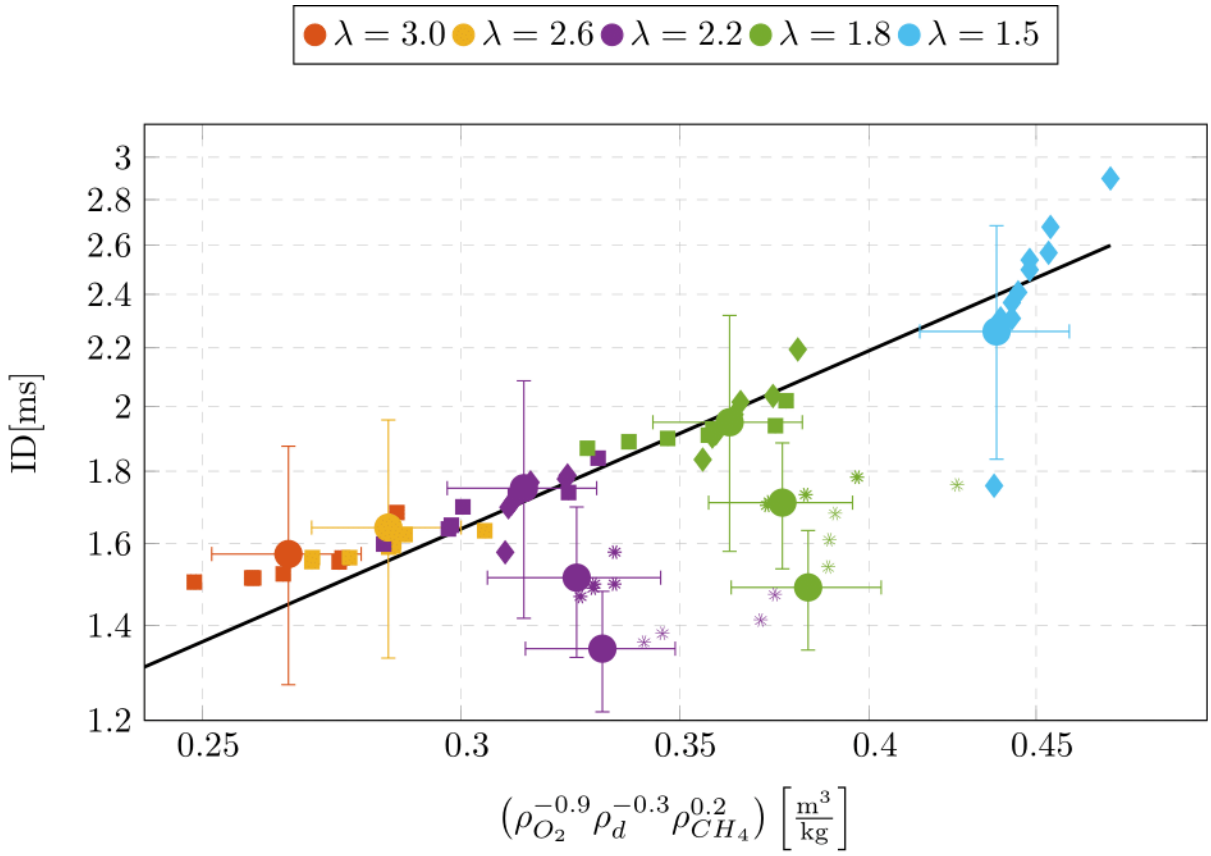

Fig. 6 ID against a suggested effective concentration.

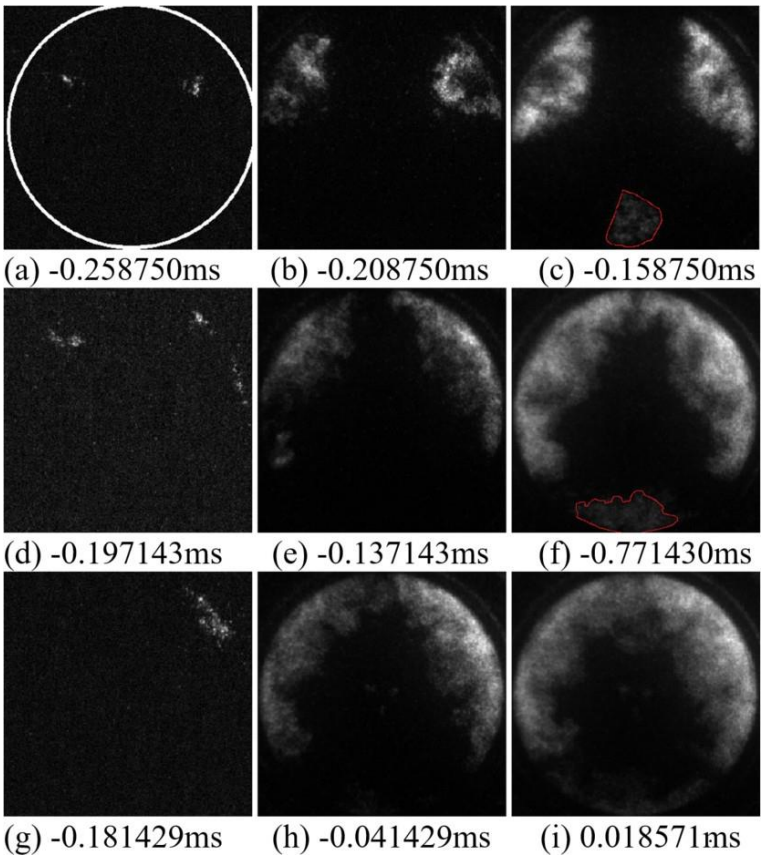

Fig. 7 OH* chemiluminescence temporal evolution at ignition for diesel (up), λ = 3.0 (middle) and λ = 1.8 (down). Origin of times (0 ms) corresponds to TDC. Subfigures (a), (d) and (g) correspond to the earliest time stamp with any area showing any OH* chemiluminescence signal. Origin of times (0 ms) corresponds to TDC. Subfigures (c), (f) and (i) relate to the first frame that shows any OH* luminosity corresponding to the spray plume that aims at the bottom of the cylinder.

4.2 Ignition Sequence Visualization

OH* chemiluminescence snapshots in Fig. 7 might give an insight of the ignition. Figs. 7a-7c represent the ignition of the 12 mg diesel injection in a pure air ambient whereas Figs. 7d-7f and Figs. 7g-7i were recorded from the leanest and richest air-natural-gas mixtures of the 12 mg injection respectively (λ = 3.0 and λ = 1.8). Time in labels correspond to ms before (negative) or after (positive) top dead centre. In the diesel combustion case, an asymmetry can be detected: First two hot spots appear a distance about the lift-off length from the injector tip [24] before the spray reaches the cylinder wall, and later the bottom spray ignites. This could be an indicator of a temperature gradient in the combustion chamber. For both dual fuel cases, ignition visibly takes place near the walls. If the reader draws his or her attention to the areas limited by a red border in Figs. 7c and 7f he or she will notice it is hard to tell an ignition area for the coldest spray in Fig. 7i.

Ignition in the richest case takes longer but the most noticeable difference is that even though the coldest spray that aims at the bottom of the combustion chamber is able to ignite by itself in the λ = 3.0, it does not seem capable of doing so before the premixed flame front from the other two sprays spreads though the bottom wall in the richest experiment (λ = 1.8). Mixture formation plays a major role here. As portrayed by Riess et al. [31, 32] spray behavior in terms of evaporation and heating of the mixture until it reaches self-ignition conditions is overall limited by the mass ratio even at penetration depths as small as 3 mm. Due to the methane flame inhibitor nature, the diesel fuel

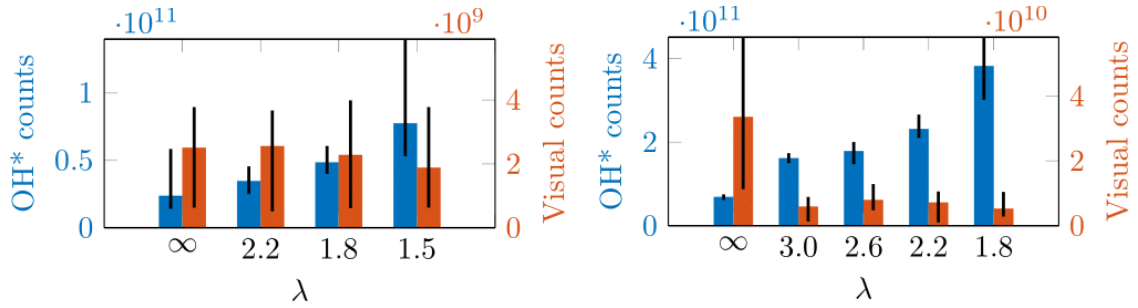

(a) Long injection of 12.2 mg (b) Short injection of 6.7 mg

Fig. 8 Total counts in camera sensor for OH* and natural flame luminosity.

requires higher temperature and more air entrainment to ignite. In example, for the pure diesel case first ignition occurs about 15mm from the cylinder wall, while in DF combustion it happens once the spray cone has reached the cylinder wall and it is spreading through it. From Ref. [20] we can estimate that spray ignition requires more than twice air entrainment for an ambient blend of $\lambda = 1.8$ than for a pure air atmosphere. Knocking or PREMIER [33] auto ignition modes of the natural gas were not appreciated in experiments of $\lambda = 1.5$ with a 6.7 mg diesel injection.

5. Optical Signals

The light emitted by a diesel flame is dominated by soot incandescence. As summarized by Azimov et al. [33]: Previous shock tube measurements have shown that continuum emission at a wavelength above 650 nm is due to either young soot particles or large hydrocarbon molecules and the maximum emissive power of soot particles, estimated as a black body, occurs in the range of about 680-1,100 nm. This leads Azimov et al. [33] to attribute emission luminosity above 650 nm observed to the luminosity from soot particles formed during the combustion of the injected diesel fuel concurrently with that of the natural gas mixture. Following this philosophy, since the optical configurations for all operation experiments in this work were the same, it is feasible to compare the spatially integrated natural luminosity for different conditions as a qualitative indicator of the soot emission [34]. Red color bars in Fig. 8 represent, on average for 8 experiments, the total number of counts in the visual camera. Black vertical lines indicate the spread (minimum to maximum total cumulative counts) among the 8 experiments. On the other hand, blue bars stand for the total cumulative counts in the OH* imaging as a qualitative indicator of the methane combustion. Both for the short and long pilot diesel injection, total OH* counts systematically increase as the ambient methane concertation does. For the long diesel injection, there is a noticeable drop in the visual signal between the diesel case ($\lambda = \infty$) and the four dual fuel cases. For the short injection, with a much smaller soot production this gap is not so clear. This is due to the lower PHRR measured in agreement with Fig. 11 of Srna et al. [7].

6. Conclusions

(i) Natural gas reactivity plays a fundamental role in dual fuel combustion acting as flame inhibitor. Thus, diesel requires more air entrainment to ignite. As a result, ID holds forth when increasing the content in ambient natural gas.

(ii) Air-natural gas lean mixtures may produce quenching achieving a poor combustion efficiency. Richer ambient blends, longer injections and a higher intake temperature or compression ratio will help to achieve a complete combustion, though the risk of knocking increases.

(iii) For small variations in the natural gas concentration, an Arrhenius-type equation could be used to trim a determinate dual fuel engine working

with a certain natural gas composition to provide with a guess of the ID.

(iv) Recirculation zones generated during the pilot fuel injection might help to bring new natural gas-ambient air pre-mixture improving the combustion that otherwise would only relay on a diffusive flame front spreading mechanism.

(v) Shorter or longer injection strategies do not vary ID above the data dispersion yet they influence in the PHRR and the combustion efficiency.

(vi) Dual fuel cases present a really low propensity to soot production.

Funding

The work has been financed by the European Research Council with a “Horizon Europe: Marie Skłodowska-Curie Actions” grant and it can be disseminated freely.

Acknowledgments

Authors gratefully acknowledge the EU H2020 founding received as under MSCA Grant Agreement No 861002. Website: https://edem-itn.eu/.

Conflict of Interests

The authors declare that there is no conflict of interest regarding the study that is being presented. The work has not been published before and it is not being sent to any other Journal.

References

[1] Reitz, R. D., and Duraisamy, G. 2015. “Review of High Efficiency and Clean Reactivity Controlled Compression Ignition (RCCI) Combustion in Internal Combustion Engines.” *Prog. Energy Combust. Sci.* 46: 12-71. doi: 10.1016/j.pecs.2014.05.003.

[2] Ma, S., Zheng, Z., Liu, H., Zhang, Q., and Yao, M. 2013. “Experimental Investigation of the Effects of Diesel Injection Strategy on Gasoline/Diesel Dual-Fuel Combustion.” *Appl. Energy* 109: 202-12. doi: 10.1016/j.apenergy.2013.04.012.

[3] Russwurm, T., Peter, A., Strauss, L., Riess, S., and Wensing, M. 2022. “Investigations on an Active Pre-chamber Ignition System in a Combustion Chamber.” *Int. J. Engine Res.* 24 (6): 1468-0874. doi: 10.1177/14680874221120140.

[4] Desantes Fernandez, J. M., Lopez, J. J., Garc´ıa-Oliver, J, M., and Lopez-Pintor, D. 2017. “A Phenomenological Explanation of the Autoignition Propagation under HCCI Conditions.” *Fuel* 206: 43-57. doi: 10.1016/j.fuel.2017.05.075.

[5] Cho, S., and Lopez-Pintor, D. 2022. “Understanding the Effects of Doping a Regular E10 Gasoline with EHN in an HCCI Engine: Experimental and Numerical Study.” *Fuel* 329: 125456. doi: 10.1016/j.fuel.2022.125456.

[6] Ma, F., Wang, J., Wang, Y., Wang, Y., Li, Y., Liu, H., and Ding, S. 2008. “Influence of Different Volume Percent Hydrogen/Natural Gas Mixtures on Idle Performance of a CNG Engine.” *Energy & Fuels* 22 (3): 1880-7. doi: 10.1021/ef7006485.

[7] Srna, A., Bolla, M., Wright, Y. M., Herrmann, K., Bombach, R., Pandurangi, S. S., Boulouchos, K., and Bruneaux, G. 2019. “Effect of Methane on Pilot-Fuel Auto-Ignition in Dual-Fuel Engines.” *Proc. Combust. Inst.* 37 (4): 4741-9. doi: 10.1016/j.proci.2018.06.177.

[8] Mikulski, M., Balakrishnan, P. M., and Hunicz, J. 2019. “Natural Gas-Diesel Reactivity Controlled Compression Ignition with Negative Valve Overlap and In-Cylinder Fuel Reforming.” *Appl. Energy* 254: 113638. doi: 10.1016/j.apenergy.2019.113638.

[9] Merts, M., Derafshzan, S., Hyvo¨nen, J., Richter, M., Lund-gren, M., and Verhelst, S. 2021. “An Optical Investigation of Dual Fuel and RCCI Pilot Ignition in a Medium Speed Engine.” *JFUECO* 9: 100037. doi: 10.1016/j.jfueco.2021.100037.

[10] Chen, Z., Wang, L., Wang, X., Chen, H., Geng, L., and Gao, N. 2022. “Experimental Study on the Effect of Water Port Injection on the Combustion and Emission Characteristics of Diesel/Methane Dual-Fuel Engines.” *Fuel* 312: 122950. doi: 10.1016/j.fuel.2021.122950.

[11] Bernd, O. 2001. “Dieselmotorische Kraftstoffzerst aubung und Gemischbildung mit Common-Rail Einspritzsyste-men.” PhD thesis, Technical University of Munich. https://testem.de/.

[12] Sven Michael, E. 2003. “Visualisierung der dieselmo-torischen Verbrennung in einer schnellen Kompressionsmas-chine.” PhD thesis, Technical University of Munich. https://testem.de/.

[13] Desantes Fernandez, J. M., Lo´pez, J. J., Garc´ıa Oliver, J. M., and Lo´pez Pintor, D. 2017. “Experimental Validation and Analysis of Seven Different Chemical Kinetic Mechanisms for *n*-Dodecane Using a Rapid Compression-Expansion Machine.” *Combust Flame* 182: 76-89. doi: 10.1016/j.combustflame.2017.04.004.

[14] Desantes-Fernandez, J. M., Garc´ıa-Oliver, J. M., Vera-Tudela-Fajardo, W., Lopez Pintor, D., Schneider, B., and

Boulouchos, K. 2016. "Study of Ignition Delay Time and Generalization of Auto-Ignition for PRFs in a RCEM by Means of Natural Chemiluminescence." *Energy Convers. Manag.* 111: 217-28. doi: 10.1016/j.enconman.2015.12.052.

[15] Kobori, S., Kamimoto, T., and Aradi, A. A. 2000. "Study of Ignition Delay of Diesel Fuel Sprays." *Int. J. Engine Research* 1 (1): 29-39. doi: 10.1243/1468087001545245.

[16] Srna, A., Bruneaux, G., von Rotz, B., Bombach, R., Herrmann, K., and Boulouchos, K. 2018. "Optical Investigation of Sooting Propensity of *n*-Dodecane Pilot/Lean-Premixed Methane Dual-Fuel Combustion in a Rapid Compression-Expansion Machine." *SAE Int. J. Engines* 11 (6): 1049-68. doi: 10.4271/2018-01-0258.

[17] Srna, A., von Rotz, B., Herrmann, K., Boulouchos, K., and Bruneaux, G. 2019. "Experimental Investigation of Pilot-Fuel Combustion in Dual-Fuel Engines, Part 1: Thermodynamic Analysis of Combustion Phenomena." *Fuel* 255: 115642. doi: 10.1016/j.fuel.2019.115642.

[18] Srna, A., von Rotz, B., Bolla, M., Wright, Y. M., Herrmann, K., Boulouchos, K., and Bruneaux G. 2019. "Experimental Investigation of Pilot-Fuel Combustion in Dual-Fuel Engines, Part 2: Understanding the Underlying Mechanisms by Means of Optical Diagnostics." *Fuel* 255: 115766. doi: 10.1016/j.fuel.2019.115766.

[19] Peter, A., Fru¨hhaber, J., Schuh, S., Lauer, T., Winter, F., Priesching, P., and Wensing, M. 2018. "Flame Quenching during Dual-Fuel Operation Investigated in EXPEriments and Simulation." *In Conference on Thermo- and Fluid Dynamic Processes in Direct Injection Engines (THIESEL).*

[20] Naber, J. D., and Siebers, D. L. 1996. "Effects of Gas Density and Vaporization on Penetration and Dispersion of Diesel Sprays." *SAE Trans.* 105 (3): 82-111. doi: 10.4271/960034.

[21] Wissink, M., and Reitz, R. 2016. "Exploring the Role of Reactivity Gradients in Direct Dual Fuel Stratification." *SAE International J. Engines* 9 (2): 1036-48. doi: 10.4271/2016-01-0774.

[22] Sim, H., Maes, N., Weiss, L., Pickett, L., and Skeen, S. 2020. "Detailed Measurements of Transient Two-Stage Ignition and Combustion Processes in High-Pressure Spray Flames Using Simultaneous High-Speed Formaldehyde PLIF and Schlieren Imaging." *Proc Combust Inst.* 38 (4): 5713-5721. doi: 10.1016/j.proci.2020.09.026.

[23] Skeen, S. A., Manin, J., and Pickett, L. M. 2015. "Simultaneous Formaldehyde PLIF and High-Speed Schlieren Imaging for Ignition Visualization in High-Pressure Spray Flames." *Proceedings of the Combustion Institute* 35 (3): 3167-74 doi: 10.1016/j.proci.2014.06.040.

[24] Pickett, L. M., Siebers, D. L., & Idicheriay, C. A. 2005. "Relationship between Ignition Processes and the Lift-Off Length of Diesel Fuel Jets." *SAE Transactions* 114 (3): 1714-31. http://www.jstor.org/stable/44722118.

[25] Lillo, P. M., Pickett, L. M., Persson, H., Andersson, O., and Kook, S. 2012. "Diesel Spray Ignition Detection and Spatial/Temporal Correction." *SAE Int. J. Engines* 5 (3): 1330-46. doi: 10.4271/2012-01-1239.

[26] Charles, K., Westbrook, and Frederick, L. D. 1981. "Simplified Reaction Mechanisms for the Oxidation of Hydrocarbon Fuels in Flames." *Combust. Sci. Technol.* 27 (1-2): 31-43. doi: 10.1080/00102208108946970.

[27] Idicheriay, C. A., and Pickett, L. M. 2011. "Ignition, Soot Formation, and End-of-Combustion Transients in Diesel Combustion under High-EGR Conditions." *Int. J. Engine Res.* 12 (4): 376-92. doi: 10.1177/1468087411399505.

[28] Pejpichestakul, W., Ranzi, E., Pelucchi, M., Frassoldati, A., Cuoci, A., Parente, A., and Faravelli, T. 2019. "Examination of a Soot Model in Premixed Laminar Flames at Fuel-Rich Conditions." *Proceedings of the Combustion Institute* 37 (1): 1013-21. doi: 10.1016/j.proci.2018.06.104.

[29] Ranzi, E., Frassoldati, A., Stagni, A., Pelucchi, M., Cuoci, A., and Faravelli, T. 2014. "Reduced Kinetic Schemes of Complex Reaction Systems: Fossil and Biomass-Derived Transportation Fuels." *International Journal of Chemical Kinetics* 46 (9): 512-42. doi: 10.1002/kin.20867.

[30] Ranzi, E., Cavallotti, C., Cuoci, A., Frassoldati, A., Pelucchi, M., and Faravelli, T. 2015. "New Reaction Classes in the Kinetic Modeling of Low Temperature Oxidation of *n*-Alkanes." *Combustion and Flame* 162 (5): 1679-91. doi: 10.1016/j.combustflame.2014.11.030.

[31] Riess, S., Rezaei, J., Weiss, L., Peter, A., and Wensing, M. 2021. "Phase Change in Fuel Sprays at Diesel Engine Ambient Conditions: Modeling and Experimental Validation." *J. Supercrit Fluids* 173: 105224. doi: 10.1016/j.supflu.2021.105224.

[32] Riess, S., Weiss, L., Peter, A., Rezaei, J., and Wensing, M. 2018. "Air Entrainment and Mixture Distribution in Diesel Sprays Investigated by Optical Measurement Techniques." *Int. J. Engine Res.* 19 (1): 120-33. doi: 10.1177/1468087417742527.

[33] Azimov, U., Tomita, E., Kawahara, N., and Harada, Y. 2011. "Premixed Mixture Ignition in the End-Gas Region (PREMIER) Combustion in a Natural Gas Dual-Fuel Engine: Operating Range and Exhaust Emissions." *Int. J. Engine Res.* 12 (5): 484-97. doi: 10.1177/1468087411409664.

[34] Zhang, J., Jing, W., and Fang, T. 2012. "High-Speed Imaging of OH* Chemiluminescence and Natural Luminosity of Low Temperature Diesel Spray Combustion." *Fuel* 99: 226-34. doi: 10.1016/j.fuel.2012.04.031.